Earth and Planetary Science Letters 300 (2010) 367–373

Contents lists available at ScienceDirect

Earth and Planetary Science Letters

journal homepage: www.elsevier.com/locate/epsl

Compositional trends among Kaapvaal Craton garnet peridotite xenoliths and their effects on seismic velocity and density

Derek L. Schutt [a,*], Charles E. Lesher [b,1]

[a] Department of Geosciences, Colorado State University, 322 Natural Resources Building, Campus Delivery 1482, Fort Collins, CO, USA 80525-1482
[b] Department of Geology, University of California at Davis, One Shields Avenue, Davis, CA, USA 95616-8605

ARTICLE INFO

Article history:
Received 12 November 2009
Received in revised form 11 October 2010
Accepted 12 October 2010
Available online 13 November 2010

Editor: R.W. Carlson

Keywords:
composition
melt depletion
seismic velocity
lithosphere
craton
isopycnic

ABSTRACT

We examine the modes and compositions of garnet-bearing peridotite xenoliths from the Kaapvaal Craton to quantify factors governing density and seismic velocity variations within metasomatically altered cratonic mantle. Three distinct compositional trends are resolved by principal component analysis. The first reflects differences in residue composition resulting from partial melting. The second is associated with orthopyroxene (opx) enrichment, possibly due to silica addition by subduction zone fluids in the source region of the xenoliths. The third principal component reflects garnet and clinopyroxene enrichment possibly as a consequence of melt infiltration. More than half of the mineral mode variance among Kaapvaal Craton xenoliths can be accounted for by opx enrichment. Melt depletion effects can account for as much as 30% of the variance, while less than 20% of the variance is associated garnet and clinopyroxene enrichment. Using the parameterization of Schutt and Lesher (2006) we show that at cratonic mantle temperatures and pressures, orthopyroxene enrichment results in little change in bulk density (ρ_{bulk}) and shear-wave velocity (V_S), but decreases compressional wave velocities (V_P) and V_P/V_S. In contrast, melt depletion has little effect on V_P, but leads to an increase in V_S and a decrease in ρ_{bulk} and V_P/V_S. Garnet (gt) and clinopyroxene (cpx) enrichment cause an increase in ρ_{bulk}, V_P, V_S, and V_P/V_S. The isolation of the major contributions to xenolith compositional variations among the Kaapvaal Craton suite helps to reconcile seeming discrepancies among previous studies that estimate the effects of composition on mantle density and seismic velocity based on either xenolith or laboratory data. Subtle variations in these properties with the pressure of equilibration may explain some of the fine scale structure in seismic tomograms for cratonic mantle, but overall differences among peridotite lithologies can only account for at most a 2–3% change in seismic velocities. Larger changes in lithospheric seismic properties are more likely associated with temperature differences or presence of mafic or hydrated lithologies. We also find that the density effects of melt depletion are insufficient to produce cratonic mantle that is neutrally buoyant with respect to fertile convecting mantle.

1. Introduction

Seismic tomograms of the lithospheric mantle have vastly improved in accuracy in recent years due to improvements in coverage (e.g. The Earthscope Transportable Array), and techniques such as ambient noise (e.g. Bensen et al., 2007, 2008) and whole waveform (Chen et al., 2007) tomography. Given the potential of tomograms to reveal information about mantle temperature and compositional structure it is important to consider in detail how seismic velocities are influenced by these factors. While the effects of temperature are generally well constrained below about 950 °C (e.g. Faul and Jackson, 2005), the effects of composition are not. As an example, Begg et al. (2009) suggest that most of the lithospheric S-wave velocity variations within the Kaapvaal Craton are caused by composition, whereas Priestley and Tilmann (2009) attributed all of the S-wave velocity variations associated within the upper 200 km of the Kaapvaal Craton to thermal effects.

Two compositional trends are considered to have the largest influence on seismic velocities. The first reflects the changes in mantle composition due to melt generation and extraction. Residues produced by melting of peridotite are thought to be less dense than their original protoliths (fertile lherzolite) and their accumulation in the upper mantle is considered to play a critical role in stabilizing cratons (e.g. Jordan, 1979, 1981; Pollack, 1986). The seismic signature of melt depleted mantle, however, is not clear. Some studies suggest melt depletion can change S-wave velocity (V_S) by several percent (Deen et al., 2006), whereas others suggest the effects are subtle and possibly too small in magnitude to be resolved unequivocally in tomograms (Afonso et al., 2008; Lee, 2003; Matsukage et al., 2005; Schutt and Lesher, 2006; Speziale et al., 2005).

* Corresponding author. Tel.: +1 970 491 5786; fax: +1 970 491 6307.
E-mail addresses: Derek.schutt@colostate.edu (D.L. Schutt), celesher@ucdavis.edu (C.E. Lesher).
[1] Tel.: +1 530 752 9779; fax: +1 530 752 0951.

0012-821X/$ – see front matter © 2010 Elsevier B.V. All rights reserved.
doi:10.1016/j.epsl.2010.10.018

The second trend is associated with metasomatic alteration. This trend is probably best illustrated in xenoliths from the Kaapvaal Craton in southern Africa (Boyd, 1989; James et al., 2004) and to lesser extent those from the Tanzanian and Siberian Cratons (Pearson and Wittig, 2008) where elevated modal opx has been attributed to SiO_2-addition via subduction-related fluids (Kelemen et al., 1998; Kesson and Ringwood, 1989; Pearson and Wittig, 2008; Simon et al., 2007). Likewise, several authors (Deen et al., 2006; Savage and Silver, 2008; Wagner et al., 2008) have ascribed anomalous V_S and V_P/V_S regions within upper mantle beneath Africa, Chile–Argentina and western U.S. to subduction zone modification. While algorithms to calculate these properties at elevated pressures and temperatures have greatly improved in recent years (Connolly, 2005; Fullea et al., 2009; Hacker and Abers, 2004; Stixrude and Lithgow-Bertelloni, 2005), the interpretation of mantle tomograms in terms of the role of melt depletion, silica enrichment or other processes of chemical modification is incomplete.

There are several motivations for this study. The first is to see if there are any indications that compositional variations within peridotite lithologies can produce substantial velocity variations, such as the 4.5% shear-wave velocity change observed in the Kalahari Craton (Savage and Silver, 2008). A second motivation is to examine the effects of melt depletion with a dataset and method that compliments past work. Previous melt depletion studies all made simplifications by either neglecting the pressure effects on melting relations and mineral physics parameters, using simplified compositions, or extrapolating thermodynamic parameters beyond their range of compositional, temperature and pressure validity (Afonso et al., 2008; Lee, 2003; Matsukage et al., 2005; Schutt and Lesher, 2006; Speziale et al., 2005). This study examines natural mantle samples for potential equilibration pressure dependence in melt depletion trends, with our best effort at full error assessment. Our third motivation is to consider the effects of metasomatism on velocity and density. Few studies have examined the seismic velocity effects of metasomatic enrichment (Matsukage et al., 2005; Wagner et al., 2005, 2008), and none with a set of xenoliths such as that used here, where variations in metasomatic trends with rock equilibration pressure (which might be expected: Griffin et al., 1999, 2009; O'Reilly et al., 2001; O'Reilly and Griffin, 2006) are examined.

Our chief goal is to understand what compositional trends affect seismic velocity and density, by how much, and whether there are any systematic changes with depth in mantle specifically beneath the Kaapvaal Craton, South Africa. A particular challenge in working with Kaapvaal xenoliths is that they reflect not only the effects of metasomatism but carry evidence of multiple melting events (e.g. Simon et al., 2007). Thus, we cannot simply relate trends of velocity and density with xenolith composition (mineralogy and/or chemistry) to metasomatism and melt depletion. Rather, one needs to establish the dominant trends in composition by principal component analysis, which in turn can be used to evaluate the effects of changing composition along the principal component trends on velocity and density. In this way one can evaluate the magnitude of the effects on xenolith properties and only once this is accomplished speculate as to petrological causes of the dominant compositional trends, implications for lithosphere stability and interpretation of upper mantle tomograms.

2. Data and methods

Xenolith data for our analysis comes from a collection of 100+ garnet peridotite xenoliths (Boyd and Mertzman, 1987; James et al., 2004) erupted within the Kaapvaal Craton. We restrict consideration to xenoliths with equilibration pressures between 2.5 and 5.5 GPa for which adequate modal mineralogy and mineral composition are available. We exclude xenoliths with porphyclastic textures, which may have disequilibrium compositions and typically yield equilibration temperatures well above the cratonic geotherm, and those from the Premier mine exhibiting strong Fe-enrichment (Hoal, 2003). Xenolith data used for our analysis is provided as Supplementary Materials.

Compositional trends for the Kaapvaal xenolith suite are determined by principal component analysis (e.g. Behn and Kelemen, 2003) using modal data (i.e. mass proportions of ol, opx, cpx, gt, and spinel) and olivine composition in terms of $Mg\# = Mg/(Mg + Fe_{tot})$ (parameterized as a value out of 100) reported by James et al. (2004). A plot of mineral modes versus olivine Mg# is shown in Supplementary Fig. 1. As recommended by Pearson and Wittig (2008) we use only olivine core compositions; these are then multiplied by 10 to increase the variance associated with Mg# and thus force the first principal component to identify the modal trends associated with increasing Mg#. In performing principal component analysis, we plot the data in the 6-D vector space of the five mineral modes plus 10 times the Mg#, and determine the vector in this space that minimizes the variance in the data. Once this 6-D vector is found, we remove all the variance associated with this vector and calculate the next best vector that explains the modal variance, and so forth.

Pressure estimates come from previous geobarometric measurements (James et al., 2004). Where multiple estimates are available we take the average and assume a uniform pressure uncertainty of ± 0.2 GPa. Equilibration temperatures are estimated assuming xenoliths lie along a common cratonic geotherm characterized by a surface heatflow for 41 mW/m^2, crustal thickness of 41 km, crustal heat production of 0.6 $\mu W/m^3$, and mantle heat production of 0.03 $\mu W/m^3$ (Rudnick et al., 1998).

In our analysis of the data we first calculate principal component trends for the entire data set. Since melting relations in peridotite are pressure dependent and other compositional trends may also vary with pressure, the principal components are also calculated for varying pressure bins that are varied in an incremental fashion between 3.0 and 5.5 GPa. We use a bin width of 1.0 GPa that was determined empirically to be large enough to obtain robust principal components, but small enough to interrogate the pressure dependence of compositional trends. For instance, for a pressure bin centered at 3.0 GPa, only xenoliths equilibrated between 2.5 and 3.5 GPa are considered. The pressure bin is moved from 3.0 to 5.5 GPa in 0.1 GPa increments. When calculating density and velocities for xenoliths within a pressure bin we assume the center pressure of the pressure bin. Likewise, temperature is determined from our assumed geotherm for a given center pressure. By using a common pressure and temperature for all xenoliths within a particular pressure bin we are able to isolate more readily compositional effects on velocity and density from equilibration temperature and pressure.

Density and velocities at mantle temperatures and pressures are computed from the full set of xenolith compositions given by James et al. (2004) recast in terms of the forty-one mineral endmembers used the parameterization of Schutt and Lesher (2006). We assume the isentropic bulk modulus, K_s, and isothermal bulk modulus, K_T, are related by $K_S = K_T(1 + \alpha\gamma T)$ and ignore anelastic effects on velocities since the anharmonic velocity effects add to anelastic effects, and there is no clear understanding of the relationship between composition and anelasticity (e.g. Faul and Jackson, 2005). To estimate errors in the principal components and the associated physical state trends we perform a combination of Monte Carlo and bootstrapping analyses. We believe this is critical, and a limitation in previous studies, as errors in composition and mineral physics parameters can lead to large uncertainties that cannot be neglected.

Mineral mode, olivine Mg#, and mineral endmember compositions are assumed to have a one sigma error of $\pm 2\%$. For each pressure bin, we perform 20,000 iterations of bootstrap resampling (Efron and Tibshitani, 1986). The number of iterations was chosen based on numerical experiments showing that the distribution of the results converges after about 10,000 iterations. To be conservative we doubled the number of iterations.

For each bootstrapping iteration, Monte Carlo errors were added to the compositional data. Note that when a data point was used more than once within an iteration – as is common with bootstrap resampling – the same error was added to the multiple instances of the same data. Principal component analysis was then performed on the resampled data set. To calculate the effects of the principal components on density and velocity, the density, bulk and shear moduli, and V_P and V_S are calculated for each datum. The trend of the density, moduli, and velocities with length along each of the determined principal component axes was measured and is shown in the results. This presumably gives the effects of each compositional trend on these values. To attach physical significance to the trends each slope is normalized by the dominant compositional trend associated with the component.

Since outliers may substantially affect the principal components and thus the trends of density, moduli, and velocity as a function of length along the principal component axis we performed both standard least squares and a more robust analysis in which we downweight outliers. In the case of the weighted principal component calculations, data are Gaussian weighted by their distance from the center of the pressure bin using a halfwidth, $\lambda = 40$ km:

$$w = \exp\left[\frac{-(P-p_x)^2}{2*\lambda^2}\right], \quad (1)$$

where P is the pressure at the center of the pressure bin and p_x is the equilibration pressure of the individual xenolith. In calculating the relationship between principal component length and density, moduli, and velocities, both standard least squares and "Huber" weighting are used. In Huber weighting, y-values (i.e. the density, moduli, and velocities) that are more than 1-sigma away from the least squares-derived trends are downweighted by the inverse of their y-distance away from the trend in standard deviations (where the standard deviations are approximated assuming typical Gaussian statistics) (Huber, 1981). Generally the weighted and the least squares results are the same, but there are instances where this is not the case as discussed below. For brevity, we show only the least squares results.

3. Results

Before deriving compositional trends and their effects on velocity, it is instructive to examine the total effects of all compositional variations on V_P and V_S (Fig. 1). Standard deviations of the V_P and V_S scatter are 0.65% and 0.40% respectively.

Although it is likely that compositional trends vary with depth, it is informative to initially examine trends among the full set of xenoliths (Table 1; Supplementary Fig. 2). By design, Component 1 captures the major modal variations that correlate principally with ol Mg#. The absolute values are not significant as the total modal variations are normalized such that they sum to zero; however the relative magnitudes are meaningful and consistent with the general expectation of partial melting, i.e. residue depletion is associated with increasing ol Mg#, increasing modal ol and opx and decreasing modal cpx and gt. Conversely, Components 2 and 3 reflect modal variations that are independent of Mg#. Component 2 reflects the near one-for-one exchange of ol and opx, while Component 3 reflects cpx and gt addition. These three components explain 97% of the total modal variance among the xenoliths. Most of the variance, i.e., 77%, is explained by Component 2, with Components 1 and 3 explaining 9% and 12% of the variance, respectively. It may come as some surprise that the first principal component is not the dominant component as is usually the case for principal components analysis. This arises simply because we force the first component to correlate with Mg# in order to explore among the other principal components modal trends that are uncorrelated with Mg#.

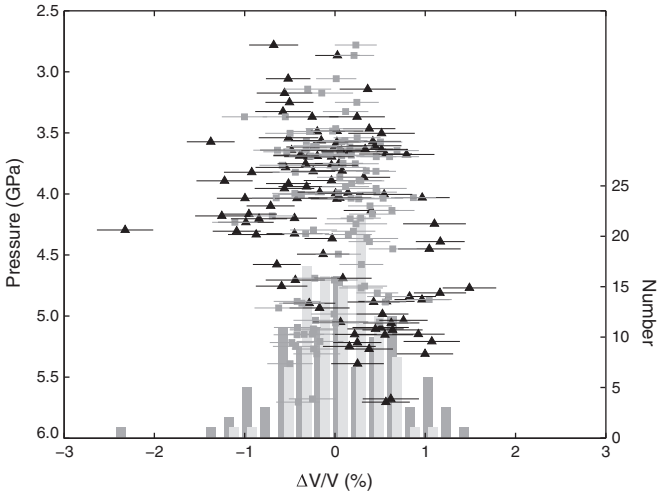

Fig. 1. Relative V_P (black triangle) and V_S (gray square) variations with estimated errors for the full set of 101 xenoliths, assuming a pressure of 4.25 GPa and temperature of 801 °C. Triangles and squares indicate individual xenolith velocities relative to the mean, and plotted by equilibration pressure (left y-axis label). Histogram at bottom of plot shows number of xenoliths (right y-axis label) falling into 0.2% wide relative velocity bins (dark gray = V_P, light gray = V_S).

The variations in principal component vector magnitude with pressure are shown in Figure 2. The number of xenoliths considered in each bin is shown in the top panel. As found for the entire data set (Table 1), the abundance of cpx and gt decreases with increasing olivine Mg# by a similar magnitude between 3 and 5.5 GPa. The variation in ol and opx mode with pressure is more complex. At low and high pressures, opx increases with Mg#, while we find little resolvable change in ol mode. In contrast, at intermediate pressures ol dominantly increases, while opx shows little change. As noted above, the second principal component predominantly reflects the tradeoff between modal opx and ol, although there is a tendency for cpx and gt to correlate with ol at lower pressure and opx at higher pressures. For the third principal component, changes in cpx and gt mode are antithetic to ol and opx, although between 4.3 and 5.3 GPa gt appears to dominate over cpx. This latter trend is not significant when the robust statistics discussed above are used.

The confidence bounds in the second principal component are generally tighter than for the other principal components, reflecting the fact that the mineral modes are most tightly correlated with distance along this principal component axis. More than half of the compositional variance is explained by Component 2, while Component 1 and Component 3 account for as much as 30% and 20% of the variance, respectively (Fig. 3). What is noteworthy is that for the Kaapvaal xenolith suite Components 1 and 3 have comparable significance, while Component 2 clearly dominates the modal variability.

Figures 4 and 5 show the relative variations in bulk density, bulk modulus and shear modulus, and V_P, V_S and V_P/V_S, respectively, with pressure for the three principal components shown in Figure 2. The

Table 1
Principal component values for full set of xenoliths.

	Component 1	Component 2	Component 3
Olivine	0.37	0.71	−0.49
Orthopyroxene	0.61	−0.70	−0.50
Clinopyroxene	−0.55	0.02	0.57
Garnet	−0.43	−0.03	0.43
Spinel	0.001	0.001	−0.001
Variance reduction	9%	77%	12%

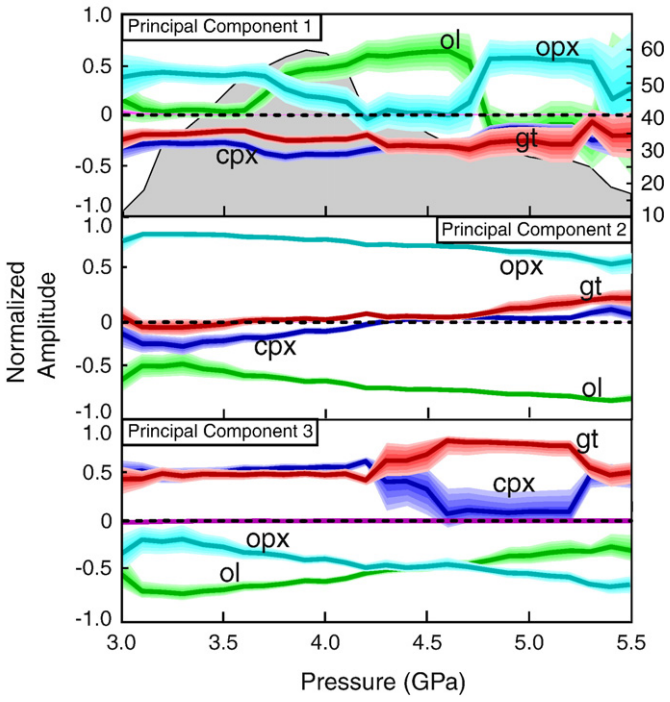

Fig. 2. The three principal components as a function of pressure. Labeled (e.g. ol, opx, etc.) colored bands indicate modal variation associated with each component, and width of band gives the 1-sigma error in the modal trend derived from error analysis. Gray figure in plot for principal component one shows the number of xenoliths in each pressure bin (number indicated in left y-axis).

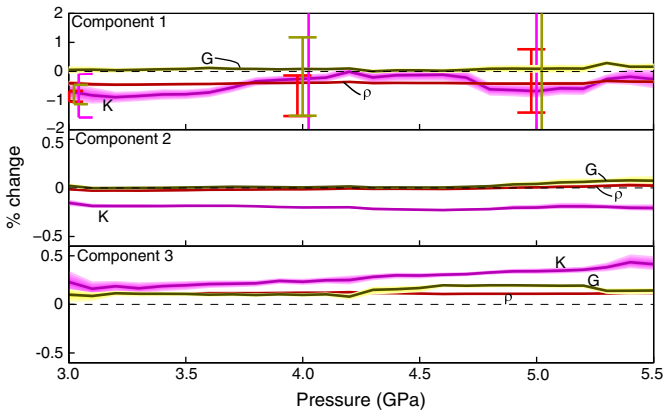

Fig. 4. Correlation between the principal components and density (red, labeled ρ), shear modulus (yellow, labeled G), and bulk modulus (purple, labeled K). Value of y-axis indicates for component one: 100*∂ln[parameter]/∂[Mg#]; component two: 100*∂ln [parameter]/∂[opx wt.%] (for change in opx wt.% along this compositional trend); component three: 100*∂ln [parameter]/∂[gt wt%] (for change in gt wt% along this compositional trend). Error bars show isobaric melt depletion effects from Schutt and Lesher (2006) along the geotherm used in this study. Error bars are slightly offset for clarity, and are for melting experiments performed at 3.5, 4.0, and 5.0 GPa.

observed ranges in these values are summarized in Table 2. In most cases, there is a clear correlation between length along the three principal components, and density, moduli, and velocities. In some cases, the trends are very tight, such as the relationship between the first principal component and density, while in other cases the trends are more obscure, such as the correlation between the first principal component and increasing bulk modulus. None of the principal components seem to have a strong correlation with shear modulus, and from 3.0 to 4.4 GPa, shear modulus variance is not well explained by any of the principal components (Fig. 6). Among the full set of xenoliths, over all pressures, shear modulus varies less than density and bulk modulus (density standard deviation = 0.73%, bulk modulus standard deviation = 2.66%, shear modulus standard deviation = 0.67%). Because of this, V_P, V_S, and V_P/V_S variations are primarily driven by variations in density and bulk modulus, and thus velocities are well correlated with principal component modal trends. V_P variance is primarily correlated with length along Component 2, and V_S variance is primarily correlated with length along Component 1.

In summary, the first principal component is associated with decreasing density and increasing V_S; the second component has little effect on density but a strong effect on V_P; the third principal component has significant correlation with increasing density, but not a clear effect on velocity. The correlations between the principal components and the various parameters generally are successful in explaining the variance in the xenolith velocities (Fig. 6). In particular, the first principal component explains most of the density and V_S variation among the xenoliths, and the second component explains much of the bulk modulus and V_P variation. The shear modulus variation, which is rather small, is not well explained by the principal components.

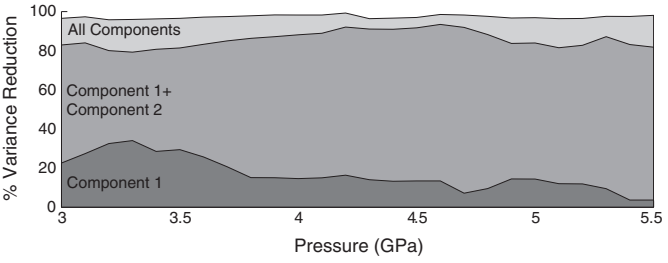

Fig. 3. Cumulative modal variance reduction for the principal components one (dark gray), two (medium gray), and three (light gray).

4. Discussion

It is worth noting that principal components are constrained to be orthogonal, in this case in the 6-D vector space of the five mineral modes examined plus olivine Mg#. Thus, one must be careful to separate the objectively found trends from our subjective interpretation of the cause of the trends.

The first component is designed to be the correlation between the mineral modes and increasing olivine Mg#. Since olivine Mg# was measured in the center of olivine grains (James et al., 2004), and the

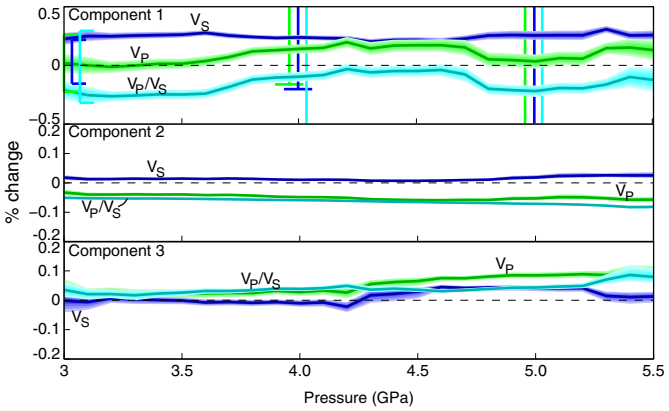

Fig. 5. Correlation between the principal components and V_P (green), V_S (blue), and V_P/V_S (cyan). Value of y-axis has the same definition as in Figure 4, except in this case [parameter] refers to V_P, V_S, and V_P/V_S. Error bars are also as in Figure 4.

Table 2
Range of correlation slopes for the three principal components over all pressures shown in Figure 2 (where xenoliths are analyzed by moving pressure bins) for density, moduli and velocity. Slopes are given as % relative change in the parameter, as a function of change in a compositional value (Mg#, opx wt.%, and gt wt.%) that varies significantly along the principal component. For instance, in Figure 2, density varies by about −0.45% to −0.32% per unit increase in Mg# in principal component 1.

Parameter	Density	Bulk modulus	Shear modulus	V_P	V_S	V_P/V_S
Component 1	−0.45(4) to −0.32%	−0.9(2) to 0.0%	0.01(8) to 0.29%	−0.01(5) to 0.20%	0.20(3) to 0.31%	−0.26(5) to −0.03%
Component 2	−0.029(8) to 0.027%	−0.29(2) to −0.15%	−0.00(1) to 0.08%	−0.059(5) to −0.33%	0.007(4) to −0.026%	−0.083(2) to −0.051%
Component 3	0.10(1) to 0.12%	0.16(4) to 0.43%	0.08(3) to 0.20%	0.01(2) to 0.10%	−0.02(2) to 0.04%	0.02(1) to 0.09%

Error given 1 − σ error for that parameter and component, averaged over all pressures.

Fe-rich Premier mine xenoliths discarded, it is likely that olivine Mg# is a reasonable proxy for melt depletion, and thus the first component is the modal evolution associated with increasing amounts of melt depletion. Although Bernstein et al. (2007) suggest that on average cratonic mantle has been melted to opx exhaustion, they also note a correlation between Mg# and mineral modes, as shown here. Isobaric partial melting experiments show opx and ol should increase with increasing Mg#, whereas gt and cpx decrease (e.g. Baker and Stolper, 1994; Lesher et al., 2003; Schutt and Lesher, 2006; Walter, 1998), in agreement with the trends for Component 1. However, for much of the pressure range sampled, opx increases more than ol. It is difficult to discern whether this is significant, since these rocks have undergone multiple polybaric fractional melting events and it is unlikely that the trends found in these rocks will be identical to isobaric melting experiments. It is also possible that Mg# is altered by metasomatism as well as melting; although it is difficult to envision metasomatic effects that would cause both Mg# and modal opx to increase together with a decrease in modal gt and cpx. Moreover, the xenoliths we consider were equilibrated above the melt-metasomitized layer discussed by Griffin et al. (2009), where Fe, Al, and Ca addition has been proposed.

The second principal component shows the dominant modal trends remaining after essentially all the modal correlations with Mg# have been isolated. This is similar to the opx enrichment trend widely noted by Kaapvaal researchers, in which olivine reacts with silica-rich fluid/melt (perhaps derived from the slab) to produce opx (Kelemen et al., 1998; Kesson and Ringwood, 1989; Pearson and Wittig, 2008; Simon et al., 2007). Our principal component analysis identifies a third component, most evident at lower pressures, in which garnet and clinopyroxene increase and olivine and orthopyroxene decrease. This latter trend accounts for 10–20% of the modal variance and, as proposed by Pearson and Wittig (2008), may reflect late addition or infiltration of melt.

Before discussing the effects of composition on density and velocity, it needs to be stressed that variations in Kaapvaal xenolith

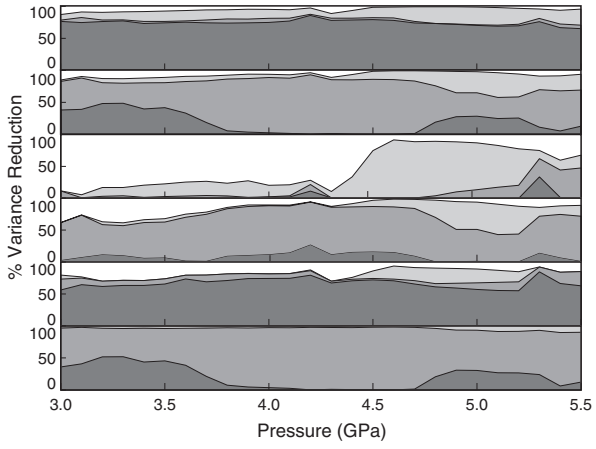

Fig. 6. Cumulative variance reduction of each of the parameters. Plots from top to bottom show variance reduction for the parameters of density, bulk modulus, shear modulus, V_P, V_S, and V_P/V_S. Variation in gray shading indicates variance reduction for principal components one (dark gray), two (medium gray) and three (light gray).

compositions can only account for about 2% variation in V_P and V_S (Fig. 1). This stands in contrast to the ~16% V_S variations observed in the lithosphere worldwide (Bensen et al., 2009). If the compositional variations observed in the Kaapvaal Craton are reasonably representative of peridotite lithologies throughout the lithospheric mantle, then it is clear that peridotite compositional variations do not play a major role in producing observed velocity anomalies. Probably most of the cause of upper mantle velocity variations are due to variations in temperature or melting (e.g. Goes and van der Lee, 2002), although significant velocity effects have been ascribed to composition (Artemieva, 2009; Deen et al., 2006; Savage and Silver, 2008). Notably, Savage and Silver (2008) imaged a 4.5% V_S drop beneath the relatively thermally homogeneous Kalahari Craton. If compositional variations are the cause of this V_S perturbation, then it is likely that this is due to: 1) more extreme compositional changes (peridotite to mafic lithologies), 2) the addition of water or volatiles (Jacobsen et al., 2008, 2009) or 3) variations in anelasticity produced by variations in composition (Sundberg and Cooper, 2010). On the other hand, a percent or so velocity variation is well within the bounds of what a tomographic study can resolve. So if other effects, such as thermal variations, can be constrained, then it is conceivable that tomograms could be used to map compositional variations within the mantle. For instance, composition could be sufficient to produce the 1–2% variations in V_S tomographically imaged in the upper mantle under the Kaapvaal Craton (Priestley and Tilmann, 2009).

This study resolves some of the seeming discrepancies between past examinations of the velocity effects of melt depletion. We find that there is a small but resolvable correlation between Mg# and S-wave velocity, and there is little pressure effect on the trend. This is consistent with and complements the findings of (Afonso et al., 2010; Lee, 2003; Matsukage et al., 2005; Schutt and Lesher, 2006) For instance, Lee (2003) reports a $dVS/d\mathrm{Mg\#} = 0.0143 \pm 0.0009$ km/s. We find $dV_S/d\mathrm{Mg\#} = 0.013 \pm 0.001$ km/s using the whole set of 101 xenoliths, a pressure of 4.25 GPa, and a temperature of 801 °C (the temperature we calculate along the geotherm at this pressure). Matsukage et al. (2005) report $d\ln V_S/d\mathrm{Mg\#}$ values of 0.0088 to −0.0018. Likewise, the value of $d\ln V_S/d\mathrm{Mg\#}$ using our entire data set is 0.0026 and well within this range. This comparison is not strictly accurate, as Matsukage et al. (2005) used whole rock Mg#, whereas we use olivine Mg#. Calculations using Perple_X (Connolly, 1990) by Afonso et al. (2010) yield $d\ln V_S/d\mathrm{Mg\#} = 0.00335$ and $d\ln V_P/d\mathrm{Mg\#} = 0.00166$ for garnet peridotite xenoliths. These values fall within the range shown in Figure 5, although our values (Table 3) tend to be lower.

The trend for opx enrichment derived from our principle component analysis on seismic velocities cannot be directly compared with similar effects found by past studies (Matsukage et al., 2005; Wagner et al., 2008). For example, Matsukage et al. (2005) considered the effects of opx and Mg# separately, whereas in our study opx varies as a function of both Mg# (the first principal component) and the opx enrichment trend (the second principal component). Further, it is difficult to directly compare to the study of Wagner et al. (2008) since they do not report derivatives; however, they do also find that V_P/V_S decreases with increasing opx abundance.

There are two notable differences between the present work and that of Schutt and Lesher (2006). The first is that the latter considered isobaric melting from laboratory experiments. This is important since

Table 3
Correlation slopes for the three principal components (1–3) of Table 1 (when all xenoliths are analyzed together, rather than by pressure bins) for density, moduli, and velocity. Slopes are given as the relative change (in %) for the parameter as a function of the corresponding change in composition [Component 1: Mg#, Component 2: opx (in wt.%), and Component 3: gt (in wt.%)] along the principal component. For instance, the value of −0.49% in the intersection of the density column and the Component 1 row is d[relative density]/*d*[Mg# variation along the Component 1 trend]. The values in square brackets give the approximate total change in the parameter along the component trend, for instance, the range of density changes due to melt depletion is about 1.26%. Note that the modal effects have been normalized to sum to zero.

Parameter	Density (%)	Bulk modulus (%)	Shear modulus (%)	V_P (%)	V_S (%)	V_P/V_S (%)
Component 1	−0.49	−0.64	0.03	+0.07	0.26	−0.19
	[−1.26]	[−1.66]	[0.07]	[0.17]	[0.67]	[−0.49]
Component 2	−0.009	−0.22	0.01	−0.06	0.01	−0.07
	[0.18]	[4.54]	[−0.22]	[1.16]	[−0.20]	[1.37]
Component 3	0.11	0.31	0.10	0.05	−0.008	0.06
	[0.56]	[1.54]	[0.48]	[0.26]	[−0.04]	[0.30]

mantle melting is clearly not isobaric and any parcel may have been melted repeatedly. In contrast, the present work considers natural variations that likely resulted from polybaric melt processes and metasomatism (Simon et al., 2007). Yet, the pressure–temperature-melting paths of Kaapvaal xenoliths are not known for certain. Thus, one study is controlled but not strictly realistic, and the other is realistic but not well controlled. Despite this, the relationships between density and velocity and Mg# found here are nearly always within the errors reported by Schutt and Lesher (2006) when the results are recalculated for a cratonic geotherm. This indeed, is the second notable difference between the two studies. Schutt and Lesher (2006) examined the effects of melting at solidus temperatures. The results from that work are slightly, but statistically different when recalculated for cratonic temperatures, and fit the trends found in the xenoliths (Figs. 4 and 5).

An intriguing difference between these results and Schutt and Lesher (2006) is that no pressure dependence is found in the effects of melt depletion. This may imply that xenoliths that have equilibrated at different pressures have undergone similar melting processes, which may support a subduction-related origin for the depleted mantle beneath the Kaapvaal Craton (e.g. Pearson and Wittig, 2008), although a more rigorous evaluation of polybaric melting on density is required to test this hypothesis.

It is widely believed that the relatively cold cratonic upper mantle will drip away into the deeper Earth if it is not positively or neutrally buoyant with respect to the convecting asthenosphere at similar depths (Jordan, 1979, 1981; Pollack, 1986). Thus, the density effects of melt depletion are thought to counteract the density effects of temperature. Quantitatively this implies that $-\Delta\rho/\rho = \alpha_v \Delta T$, where $-\Delta\rho/\rho$ is the relative density effects of melt depletion with respect to fertile mantle, α_v is volumetric thermal expansivity, and ΔT is the temperature difference between asthenosphere and cratonic mantle. In the strictest sense this *isopycnic hypothesis* is thought to hold at every depth. Thus, for example, at 4.25 GPa, the temperature difference between cratonic and asthenospheric mantle is >530 °C (assuming a cratonic temperature of ~800 °C and a conservative potential temperature of 1280 °C (Herzberg et al., 2007; Rudnick et al., 1998)). The average thermal expansivity between cratonic and asthenospheric mantle at these pressure and temperature conditions is $\alpha_v = 3.42 \times 10^{-5}$ (Schutt and Lesher, 2006), so $\alpha_v \Delta T = \sim 1.8\%$. This implies cold fertile cratonic mantle would be 1.8% denser than hot fertile asthenospheric mantle. For depleted cratonic mantle to be isopycnic, the chemical effects of melt depletion $-\Delta\rho/\rho$ must be equivalent; however, Table 3 shows that the full range of density variations among the xenoliths due to melt depletion is $-\Delta\rho/\rho = \sim 1.26\%$. Hence, if the xenoliths represent the full range of density effects due to melt depletion between fertile and cratonic mantle, then the Kaapvaal mantle at 4.25 GPa and above must be heavy with respect to fertile asthenosphere. If this is indeed the case then the long term stability of cratonic mantle may have more to do with its high viscosity than its density. The neutral geoid signal (Shapiro et al., 1999) could be explained by deeper cratonic mantle being positively buoyant with respect to asthenosphere. Afonso et al. (2008) advanced a similarly stratified model consistent with geoid observations.

5. Summary

Among garnet peridotite xenoliths from the Kaapvaal Craton, three dominant compositional trends are observed and their effects on velocity and density quantified: 1) melt depletion, 2) orthopyroxene enrichment, and 3) garnet and clinopyroxene enrichment. The most significant effects we find from compositional variations can be summarized as follows: 1) melt depletion decreases density; 2) melt depletion increases V_S; 3) opx enrichment decreases V_P; and 4) gt/cpx enrichment increases density. We find that the total effect of melt depletion on density is ~1.2% and on V_S is ~0.7%. The total effect of opx enrichment on V_P is ~1.2%, while the total effect of gt/cpx enrichment on density is ~0.6%. The isolation of the major contributions to xenolith compositional variations among the Kaapvaal Craton suite helps to reconcile discrepancies among previous studies that estimate the effects of composition on mantle density and seismic velocity based on either xenolith or laboratory data. Subtle variations in these properties with the pressure of equilibration may explain fine scale structure in seismic tomograms for cratonic mantle, but overall differences among peridotite lithologies can only account for at most a 2–3% change in seismic velocities. Larger changes in lithospheric seismic properties are more likely associated with temperature differences and/or basaltic and hydrated lithologies. These results further indicate that Kaapvaal Craton lithosphere is not isopycnic, but rather denser than asthenospheric mantle suggesting that it owes its persistence to its high viscosity.

Supplementary materials related to this article can be found online at 10.1016/j.epsl.2010.10.018.

Acknowledgements

We thank editor Rick Carlson, and reviewers Juan Carlos Afonso and Nina Simon for their helpful comments, and the NSF Geophysics and Petrology and Geochemistry programs for grants EAR-0409538 (DLS) and EAR-0409375 (CEL).

References

Afonso, J.C., Fernandez, M., Ranalli, G., Griffin, W.L., Connolly, J.A.D., 2008. Integrated geophysical–petrological modeling of the lithosphere and sublithospheric upper mantle: methodology and applications: Geochem. Geophys. Geosys. 9, Q05008. doi:10.1029/2007GC001834.

Afonso, J.C., Ranalli, G., Fernandez, M., Griffin, W.L., O'Reilly, S.Y., Faul, U., 2010. On the Vp/Vs-Mg# correlation in mantle peridotites: implications for the identification of thermal and compositional anomalies in the upper mantle. Earth Planet. Sci. Lett. 289, 606–618. doi:10.1016/j.epsl.2009.12.005.

Artemieva, I.M., 2009. The continental lithosphere: reconciling thermal, seismic, and petrologic data. Lithos 109, 23–46.

Baker, M.B., Stolper, E.M., 1994. Determining the composition of high-pressure mantle melts using diamond aggregates. Geochim. Cosmochim. Acta 58, 2811–2827.

Begg, G.C., Griffin, W.L., Natapov, L.M., O'Reilly, S.Y., Grand, S.P., O'Neill, C.J., Hronsky, J.M.A., Djomani, Y.P., Swain, C.J., Deen, T., Bowden, P., 2009. The lithospheric architecture of Africa: seismic tomography, mantle petrology, and tectonic evolution. Geosphere 5, 23–50.

Behn, M.D., Kelemen, P.B., 2003. Relationship between seismic P-wave velocity and the composition of anhydrous igenous and meta-igneous rocks. Geochem. Geophys. Geosys. 4. doi:10.1029/2002gc000393.

Bensen, G.D., Ritzwoller, M.H., Barmin, M.P., Levshin, A.L., Lin, F., Moschetti, M.P., Shapiro, N.M., Yang, Y., 2007. Processing seismic ambient noise data to obtain reliable broad-band surface wave dispersion measurements. Geophys. J. Int. 169, 1239–1260 10.1111/j.1365-246X.2007.03374.x.

Bensen, G.D., Ritzwoller, M.H., Shapiro, N.M., 2008. Broadband ambient noise surface wave tomography across the United States. J. Geophys. Res. 113, B05306. doi:10.1029/2007jb005248.

Bensen, G.D., Ritzwoller, M.H., Yang, Y., 2009. A 3-D shear velocity model of the crust and uppermost mantle beneath the United States from ambient seismic noise. Geophys. J. Int. 177, 1177–1196 10.1111/j.1365-246X.2009.04125.x.

Bernstein, S., Kelemen, P.B., Hanghoj, K., 2007. Consistent olivine Mg# in cratonic mantle reflects Archean mantle melting to the exhaustion of orthopyroxene. Geology 35, 459–462. doi:10.1130/g23336a.1.

Boyd, F.R., 1989. Compositional distinction between oceanic and cratonic lithosphere. Earth Planet. Sci. Lett. 96, 15–26.

Boyd, F.R., Mertzman, S.A., 1987. Composition and structure of the Kaapvall lithosphere, southern Africa. In: Mysen, B.O. (Ed.), Magmatic Processes: Physiochemical Principles: University Park, PA, Geochemical Society, pp. 13–24.

Chen, P., Zhao, L., Jordan, T.H., 2007. Full 3D tomography for the crustal structure of the Los Angeles region. Bull. Seism. Soc. Am. 97, 1094–1120.

Connolly, J.A.D., 1990. Multivariable phase-diagrams — an algorithm based on generalized thermodynamics. Am. J. Sci. 290, 666–718.

Connolly, J.A.D., 2005. Computation of phase equilibria by linear programming: a tool for geodynamic modeling and its application to subduction zone decarbonation. Earth Planet. Sci. Lett. 236, 524–541.

Deen, T.J., Griffin, W.L., Begg, G., O'Reilly, S.Y., Natapov, L.M., Hronsky, J., 2006. Thermal and compositional structure of the subcontinental lithospheric mantle: derivation from shear wave seismic tomography. Geochem. Geophys. Geosys. 7.

Efron, B., Tibshitani, R., 1986. Bootstrap methods for standard errors, confidence intervals, and other measures of statistical accuracy. Stat. Sci. 1, 54–77.

Faul, U.H., Jackson, H.R., 2005. The seismological signature of temperature and grain size variations in the upper mantle. Earth Planet. Sci. Lett. 234, 119–134.

Fullea, J., Afonso, J.C., Connolly, J.A.D., Fernandez, M., Garcia-Castellanos, D., Zeyen, H., 2009. LitMod3D: an interactive 3-D software to model the thermal, compositional, density, seismological, and rheological structure of the lithosphere and sublithospheric upper mantle. Geochem. Geophys. Geosys. 10.

Goes, S., van der Lee, S., 2002. Thermal structure of the North American uppermost mantle inferred from seismic tomography. J. Geophys. Res. 107.

Griffin, W.L., O'Reilly, S.Y., Afonso, J.C., Begg, G.C., 2009. The composition and evolution of lithospheric mantle: a re-evaluation and its tectonic Implications. J. Petrol. 50, 1185–1204. doi:10.1093/petrology/egn033.

Griffin, W.L., O'Reilly, S.Y., Davies, R., Kivi, K., van Achterbergh, E., Natapov, L.M., Doyle, B.J., Ryan, C.G., Pearson, N.J., 1999. Layered mantle lithosphere in the Lac de Gras area, Slave craton: Composition, structure and origin. J. Petrol. 40, 705–727.

Hacker, B.R., Abers, G.A., 2004. Subduction Factory 3: an Excel worksheet and macro for calculating the densities, seismic wave speeds, and H_2O contents of minerals and rocks at pressure and temperature. Geochem. Geophys. Geosys. 5, 7.

Herzberg, C., Asimow, P.D., Arndt, N., Niu, Y.L., Lesher, C.M., Fitton, J.G., Cheadle, M.J., Saunders, A.D., 2007. Temperatures in ambient mantle and plumes: Constraints from basalts, picrites, and komatiites. Geochem. Geophys. Geosys. 8. doi:10.1029/2006gc001390.

Hoal, K.O., 2003. Samples of Proterozoic iron-enriched mantle from the Premier kimberlite: Slave-Kaapvaal Workshop, 5–9 September 2001, 71, pp. 259–272.

Huber, P., 1981. Robust Statistics. John Wiley & Sons, Hoboken, NJ, p. 322.

Jacobsen, S.D., Jiang, F.M., Mao, Z., Duffy, T.S., Smyth, J.R., Holl, C.M., Frost, D.J., 2008. Effects of hydration on the elastic properties of olivine. Geophys. Res. Lett. 35. doi:10.1029/2008gl034398.

Jacobsen, S.D., Jiang, F.M., Mao, Z., Duffy, T.S., Smyth, J.R., Holl, C.M., Frost, D.J., 2009. Effects of hydration on the elastic properties of olivine. Geophys. Res. Lett. 36. doi:10.1029/2009gl038660 (vol 35, L14303, 2008).

James, D.E., Boyd, F.R., Schutt, D., Bell, D.R., Carlson, R.W., 2004. Xenolith constraints on seismic velocities in the upper mantle beneath southern Africa. Geochem. Geophys. Geosys. 5. doi:10.1029/2003GC000551.

Jordan, T.H., 1979. Mineralogies, densities and seismic velocities of garnet lherzolites and their geophysical implications. In: Boyd, F.R., Meyer, H.O.A. (Eds.), The Mantle Sample; Inclusions in Kimberlites and Other Volcanics. Proceedings of the Second International Kimberlite Conference, 2. Am. Geophys. Union, Washington, D.C., United States, pp. 1–14.

Jordan, T.H., 1981. Continents as a chemical-boundary layer. Phil. Trans. A 301, 359–373.

Kelemen, P.B., Hart, S.R., Bernstein, S., 1998. Silica enrichment in the continental upper mantle via melt/rock reaction. Earth Planet. Sci. Lett. 164, 387–406.

Kesson, S.E., Ringwood, A.E., 1989. Slab mantle interactions: 1. Sheared and refertilized garnet perdotite xenoliths — samples of wadati-benioff zones. Chem. Geol. 78, 83–96.

Lee, C.T.A., 2003. Compositional variation of density and seismic velocities in natural peridotites at STP conditions: implications for seismic imaging of compositional heterogeneities in the upper mantle. J. Geophys. Res. 108. doi:10.1029/2003jb002413.

Lesher, C.E., Pickering-Witter, J., Baxter, G., Walter, M., 2003. Melting of garnet peridotite: effects of capsules and thermocouples, and implications for the high-pressure mantle solidus. Am. Mineralog. 88, 1181–1189.

Matsukage, K.N., Nishihara, Y., Karato, S., 2005. Seismological signature of chemical differentiation of Earth's upper mantle. J. Geophys. Res. 110, B12305. doi:10.1029/2004jb003504.

O' Reilly, S.Y., Griffin, W.L., Djomani, Y.H., Morgan, P., 2001. Are lithospheres forever? Tracking changes in subcontinental lithospheric mantle through time. GSA Today 11, 4–10.

O'Reilly, S.Y., Griffin, W.L., 2006. Imaging global chemical and thermal heterogeneity in the subcontinental lithospheric mantle with garnets and xenoliths: geophysical implications. Tectonophysics 416, 289–309. doi:10.1016/j.tecto.2005.11.014.

Pearson, D.G., Wittig, N., 2008. Formation of Archaean continental lithosphere and its diamonds: the root of the problem. J. Geol. Soc. 165, 895–914.

Pollack, H.N., 1986. Cratonization and thermal evolution of the mantle. Earth Planet. Sci. Lett. 80, 175–182.

Priestley, K., Tilmann, F., 2009. Relationship between the upper mantle high velocity seismic lid and the continental lithosphere. Lithos 109, 112–124. doi:10.1016/j.lithos.2008.10.021.

Rudnick, R.L., McDonough, W.F., and O'Connell, R.J., 1998, Thermal structure, thickness and composition of continental lithosphere, p. 395–411.

Savage, B., Silver, P.G., 2008. Evidence for a compositional boundary within the lithospheric mantle beneath the Kalahari craton from S receiver functions. Earth Planet. Sci. Lett. 272, 600–609. doi:10.1016/j.epsl.2008.05.026.

Schutt, D.L., Lesher, C.E., 2006. Effects of melt depletion on the density and seismic velocity of garnet and spinel lherzolite. J. Geophys. Res. 111, B05401. doi:10.1029/2003jb002950.

Shapiro, S.S., Hager, B.H., Jordan, T.H., 1999. The continental tectosphere and Earth's long-wavelength gravity field. Lithos 48, 135–152.

Simon, N.S.C., Carlson, R.W., Pearson, D.G., Davies, G.R., 2007. The origin and evolution of the Kaapvaal cratonic lithospheric mantle. J. of Petrol. 48, 589–625.

Speziale, S., F.J., TS, D., 2005. Compositional dependence of the elastic wave velocities of mantle minerals: implications for seismic properties of mantle rocks. In: Hilst, R.v.d., Bass, J.D., Matas, J., Trampert, J. (Eds.), Structure, Composition, and Evolution of Earth's Mantle, pp. 303–323. Washington, DC, AGU.

Stixrude, L., Lithgow-Bertelloni, C., 2005. Thermodynamics of mantle minerals — I. Physical properties. Geophys. J. Int. 162, 610–632. doi:10.1029/2004JB002965.

Sundberg, M., Cooper, R.F., 2010. A composite viscoelastic model for incorporating grain boundary sliding and transient diffusion creep; correlating creep and attenuation responses for materials with a fine grain size. Philos. Mag. 90, 2817–2840.

Wagner, L.S., Anderson, M.L., Jackson, J.M., Beck, S.L., Zandt, G., 2008. Seismic evidence for orthopyroxene enrichment in the continental lithosphere. Geology 36, 935–938. doi:10.1130/g25108a.1.

Wagner, L.S., Beck, S., Zandt, G., 2005. Upper mantle structure in the south central Chilean subduction zone (30° to 36° S). J. Geophys. Res. 110, 1–20.

Walter, M.J., 1998. Melting of garnet peridotite and the origin of komatiite and depleted lithosphere. J. Petrol. 39, 29–60.